Preprints of the 21st IFAC World Congress (Virtual)
Berlin, Germany, July 12-17, 2020

Real-Time Prediction of Curing Processes using Model Order Reduction

Tobias Frank * **Henrik Zeipel** * **Mark Wielitzka** *
Steffen Bosselmann * **Tobias Ortmaier** *

* *Institute of Mechatronic Systems, Leibniz University Hanover, Hanover, Germany (e-mail: tobias.frank@imes.uni-hannover.de).*

Abstract: Manifold engineering applications are directly affected by temperature. For rubber or composite curing processes, temperature distributions over time inside the compounds are crucial for chemical cross-linking reactions. Most of these reactions occur subsequently to a heating process during product cool down. Online prediction of cooling phases is performed during the actual heating process and hence, final cure status can be estimated before the actual process finishes. Therefore, mold temperatures and heating duration can be adapted in regard to current ambient conditions, and hence product quality is increased. In order to achieve longterm thermal predictions for complex product geometries, simulating nonlinear thermal finite element models is unfeasible, due to high computational effort. Hence, a prediction-model is derived from finite element analysis using matrix export, linearization, model order reduction algorithms such as rational Krylov or iterative rational Krylov and correction of operating point deviation. A special remark is given to temperature dependent boundary conditions, choice of time discretization and choice of solving algorithm, to address arising conflicting goals between execution time and simulation accuracy. Eventually, a complete process simulation is performed during the task-cycle time on a PLC control with a sufficiently high accuracy.

Keywords: Model Reduction, Prediction, Simulation, Temperature Distributions, Process Control

1. INTRODUCTION

Thermal modeling is an important step in manifold engineering applications, especially if material properties or process characteristics are directly coupled to temperature. Common examples are rubber and tire vulcanization as mentioned by Ghoreishy (2016), composite curing by Advani and Sozer (2010), heavy plate rolling described by Speicher et al. (2013, 2014), electrical components from Giacometto et al. (2016) or motor temperature management as stated by Qi et al. (2016). Sufficiently accurate transient thermal simulation results are essential during offline process planning or optimization. However, execution times and real-time requirements have to be accounted for, if online model-based control or monitoring is performed. For latter cases a conflicting goal arises between model accuracy and computation performance. Since all of the mentioned applications require formulation of distributed parameter systems, often derived from finite element analysis, handled models tend to entail large system scales and high execution times. Model simplification or coarse spatial discretization can decrease computation times, however can entail high deviations to real measurements. A different approach to address high computational effort for FEA are data-based methods such as presented by Giacometto et al. (2016). However, suitable data-sets are not always available or obtainable.

In this work, thermal modeling is performed for rubber curing processes. For chemical reactions during rubber vulcanization as well as composite curing, two process steps are essential. First, raw materials or compounds are placed inside a heated mold for a specific duration. During this heating process, final product shape is given and chemical cross-linking reactions start. Subsequently, products are taken out of the mold and cool down at ambient temperature, which can possibly endure for hours. Due to sluggish thermal behaviour of utilized materials, most of cross-linking reactions inside the materials are happening during cool down phases. This step mainly depends on ambient temperatures and air flows inside industry halls, however process operator's influence is very limited, since only mold temperature and heating duration can be controlled properly. It is of great interest to ensure a well-defined curing process, since final product quality mainly depends on homogeneous cross-linking throughout the whole cross-section. Determination of optimal curing parameters and detailed process planning is a challenging task as shown by Bosselmann et al. (2018); Aleksendrić et al. (2016); Labban et al. (2010). However, offline process planning cannot account for disturbances during actual processes. Especially ambient temperature changes in industry halls due to weather or season change, can have a significant impact on product performance and quality. Therefore, a model-based and product specific online prediction of temperature distributions during the cooling phase with current ambient properties is beneficial. Nevertheless, disturbances or changes can only be corrected during heating process, by adjusting heating duration or slightly varying mold temperatures. During heating process, frequent prediction of hour long cooling phases need

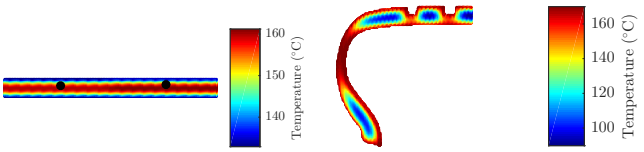

(a) rubber slab (b) tire cross-section

Fig. 1. Exemplary temperature distributions of plane rubber specimen (a) and half tire cross-section (b)

to be executed until the optimum heating duration is reached in regard to the predicted cooling trajectory. However, required thermal models derived from finite element analysis and used for process planning, intend to have high state dimensions, and hence lack of real-time capable computation. Therefore, a reduced order system description needs to be used for prediction. Section 2 describes thermal modeling process, model order reduction as well as evaluation methods. A plane rubber slab and a tire cross-section are used to exemplify the methodology. Since, cooling phases are nonlinearly affected by temperature-dependent convection and thermal radiation, a special remark is given to parameter identification and model order reduction procedure by preserving descriptive parameters. In section 3 the obtained reduced order models are eventually investigated regarding time step, solving algorithm, and nonlinear behaviour to solve for conflicting objectives between model accuracy and computation performance for real-time capability. Main challenges mentioned in this work are large system scale, state-dependent boundary conditions, inhomogeneous initial conditions occurring after heating process, restricted computational resources due to real-time requirements, and accuracy limits because of product requirements.

2. METHODS

Two different rubber composites, depicted in Figure 1, are used to exemplify a model-based real-time prediction for large scale thermal models. The first one is a rectangular shaped rubber specimen consisting of just one rubber compound with isotropic material properties. Two type-K thermocouples are placed near the centerline for validation purposes. Secondly, a tire cross section model with more than 20 components, consisting of textile and metal layers as well as different rubber compounds is evaluated. 12 virtual sensors are placed at points of interest throughout the whole cross-section, resulting in different dynamic behaviours for all output signals. Complex geometries and partly anisotropic material parameters in tires make the use of finite element modeling inevitable. In sample curing processes both examples are heated up with a subsequent cooling phase, during which most of the kinetic reactions inside rubber compounds take place. Therefore, model-based prediction of time variant temperature distributions especially during cooling is crucial for an exact determination of final state of cure at the end of process. In subsection 2.1 thermal modeling approaches are described. Since, real-time requirements have to be taken into account, a computation efficient system formulation is set up. Subsequently, subsection 2.2 describes solving algorithms and evaluation methods in regard to accuracy and execution times.

2.1 Modeling Approach

Within system domain Ω temperature distributions varying over time $T = T(\boldsymbol{z}, t))$ with $\boldsymbol{z} \in \Omega$ are calculated in regard to Fourier's law and heat equation

$$c\rho \frac{\partial}{\partial t} T = \nabla^{\mathrm{T}} \left(\lambda \nabla T \right) , \tag{1}$$

with component dependent properties: specific heat c, density ρ, and thermal conductivity λ.

Assumption 1. The system consists of spatially and temperature independent material properties within discrete components of one model.

Moreover, temperature dependent boundary conditions such as thermal radiation and convective loads affect the temperature distribution and are expressed as heat fluxes at the surface $\partial\Omega$

$$\phi_{\mathrm{conv}}(\boldsymbol{z}_{\mathrm{B}}, t) = \alpha(T) \left(T(\boldsymbol{z}_{\mathrm{B}}, t) - T_{\mathrm{amb}} \right) \quad \boldsymbol{z}_{\mathrm{B}} \in \partial\Omega \, , \tag{2}$$

$$\phi_{\mathrm{rad}}(\boldsymbol{z}_{\mathrm{B}}, t) = \epsilon\sigma \left(T(\boldsymbol{z}_{\mathrm{B}}, t)^4 - T_{\mathrm{amb}}^4 \right) . \tag{3}$$

T_{amb} denotes ambient temperature, α the film-coefficient, ϵ emission-coefficient, and σ the Stefan-Boltzmann constant, respectively. Equations (2) and (3) show a nonlinear dependency of temperature and as a result, a nonlinear function f is required to solve for temperature change over time

$$\frac{\partial}{\partial t} T = f(T, T_{\mathrm{amb}}). \tag{4}$$

Therefore, heat fluxes through the surface are defined as a combined *Robin* boundary condition

$$\phi_{\mathrm{R}}(\boldsymbol{z}_{\mathrm{B}}, t) = \alpha_{\mathrm{tot}}(T) \left(T - T_{\mathrm{amb}} \right) , \tag{5}$$

with total film-coefficient

$$\alpha_{\mathrm{tot}}(T) = \alpha_{\mathrm{conv}}(T) + \epsilon\sigma \frac{T^4 - T_{\mathrm{amb}}^4}{T - T_{\mathrm{amb}}} . \tag{6}$$

This way, nonlinear system description (4) can be transformed into a linear parameter-variant (LPV) formulation (Equation (7)), utilizing Equation (5), where all nonlinear correlations are shifted into a film-coefficient parameter α_{tot}. In order to spatially discretize resulting infinite dimensional distributed parameter system, a finite element analysis is used, since complex geometries prevent simple modeling. First-order elements generate a triangular mesh with n_{x} node temperatures $\boldsymbol{x}(t) \in \mathbb{R}^{n_{\mathrm{x}}}$ as states. Time dependency is formally neglected in the following sections. The resulting linear parameter-variant system description

$$\boldsymbol{E}\dot{\boldsymbol{x}} = \boldsymbol{A}(\boldsymbol{p})\boldsymbol{x} + \boldsymbol{B}(\boldsymbol{p})\boldsymbol{u}, \;\; \boldsymbol{x}(0) = \boldsymbol{x}_0, \tag{7}$$

$$\boldsymbol{T}_{\mathrm{S}} = \boldsymbol{C}\,\boldsymbol{x}, \tag{8}$$

consists of conductivity matrix $\boldsymbol{A} \in \mathbb{R}^{n_{\mathrm{x}} \times n_{\mathrm{x}}}$ and input matrix $\boldsymbol{B} \in \mathbb{R}^{n_{\mathrm{x}} \times n_{\mathrm{u}}}$, both containing state and input dependent parameters $\boldsymbol{p} = \boldsymbol{p}(\boldsymbol{x}, \boldsymbol{u}), \boldsymbol{p} \in \mathbb{R}^{n_{\mathrm{p}}}$ derived from the boundary conditions in (2) and (3) according to Frank et al. (2018). Furthermore, damping matrix $\boldsymbol{E} \in \mathbb{R}^{n_{\mathrm{x}} \times n_{\mathrm{x}}}$, input vector $\boldsymbol{u} \in \mathbb{R}^{n_{\mathrm{u}}}$ containing ambient temperatures, and initial temperature distribution $\boldsymbol{x}_0$ are specified. Temperature values at sensor positions $\boldsymbol{T}_{\mathrm{S}} \in \mathbb{R}^{n_{\mathrm{y}}}$ are calculated with output matrix $\boldsymbol{C} \in \mathbb{R}^{n_{\mathrm{y}} \times n_{\mathrm{x}}}$. Since system order $n_{\mathrm{x}} \gg 1000$ is of high dimension with up to multiple thousand states, model order reduction is crucial for a real-time capable online prediction. Benner et al. (2017) reviewed several reduction algorithms for linear and

parameter-dependent system descriptions. For Equation (7) linear model order reduction is not applicable, since system matrices are parameter dependent. Moreover, parametric model order reduction (PMOR) approaches can be infeasible, when the number of parameters is high and they do not remain constant. Therefore, methodology from Frank et al. (2018) is applied to generate a computation efficient system description with reduced order $q \ll n_\mathrm{x}$ and significantly reduce computation effort. Thus, the system is first linearized at an arbitrary operating point $\boldsymbol{p_0}$, leading to a linear system description

$$\begin{aligned} \boldsymbol{E}\dot{\boldsymbol{x}} &= \boldsymbol{A}|_{\boldsymbol{p_0}}\boldsymbol{x} + \boldsymbol{B}|_{\boldsymbol{p_0}}\boldsymbol{u}, \;\; \boldsymbol{x}(0) = \boldsymbol{x}_0 \\ \boldsymbol{T}_\mathrm{S} &= \boldsymbol{C}\,\boldsymbol{x}. \end{aligned} \tag{9}$$

Furthermore, inhomogeneous nonzero initial conditions $\boldsymbol{x}_0$ have to be accounted for, when cooling phases subsequent to heating processes are included in the prediction. Since initial conditions are unknown during offline modeling and determined during online processes, classical reduction algorithms can not be used to obtain an adequate reduced model. Beattie et al. (2017) propose to superpose initial condition response from an unforced system with nontrivial initial condition and forced system with zero initial condition. Subsequently, two different system formulations have to be reduced, one to model load dynamics (10) and one for initial condition response (11)

$$\boldsymbol{E}\dot{\boldsymbol{v}} = \boldsymbol{A}|_{\boldsymbol{p_0}}\,\boldsymbol{v} + \boldsymbol{B}|_{\boldsymbol{p_0}}\,\boldsymbol{u}, \qquad \boldsymbol{v}(0) = \boldsymbol{0}, \tag{10}$$

$$\boldsymbol{E}\dot{\boldsymbol{w}} = \boldsymbol{A}|_{\boldsymbol{p_0}}\,\boldsymbol{w} + \boldsymbol{X}_0\boldsymbol{\gamma}\,, \qquad \boldsymbol{w}(0) = \boldsymbol{0}\,, \tag{11}$$

$$\boldsymbol{T}_\mathrm{S} = \boldsymbol{C}\,(\boldsymbol{w} + \boldsymbol{v}), \tag{12}$$

with $\boldsymbol{X}_0 \in \mathbb{R}^{n_\mathrm{x}\times q_0}$, the columns of which form a basis for a subspace of possible initial temperature distributions $\boldsymbol{x}_0 = \boldsymbol{X}_0\,\boldsymbol{z}_0$, actual initial condition input $\boldsymbol{\gamma} = \boldsymbol{z}_0\delta(t)$, and state vectors $\boldsymbol{v}, \boldsymbol{w} \in \mathbb{R}^{n_\mathrm{x}}$. Temperatures at sensor positions $\boldsymbol{T}_\mathrm{S}$ are calculated with superposition of state vectors (12).

Dimensions of both subsystems have to be reduced by model order reduction to enable a sufficiently fast execution for real-time applications. Rational Krylov model reduction also known as moment matching from Grimme (1997) can be used to approximate transfer function moments at predefined frequency shifts. Since choice of appropriate shifts can be a challenging task, Gugercin et al. (2008) introduced the iterative rational krylov algorithm (IRKA) for $\mathcal{H}_2$ optimal transfer function approximation of linear systems. In this work, IRKA is used to calculate model order reduction projectors for linear forced and unforced dynamic, respectively. Original system order n_x is then reduced to $q_0 \ll n_\mathrm{x}$ for unforced and $q_\mathrm{u} \ll n_\mathrm{x}$ for forced dynamic.

Equations (10) and (11) are only used to calculate projection matrices to reduce system scale. However, a true linear modeling is not acceptable, due to highly nonlinear boundary conditions. As stated by Frank et al. (2018), parameter-dependent functions $\boldsymbol{g}_\mathrm{u}$ and $\boldsymbol{g}_0$ are added in both dynamics to compensate deviation between chosen initial operating point $\boldsymbol{p}_0$ and actual parameters $\boldsymbol{p}$ to account for temperature-dependent boundary conditions.

Assumption 2. State dependent parameter vector $\boldsymbol{p}$ only affects states on the domain's surface
$\boldsymbol{x}_\mathrm{B} = \boldsymbol{v}_\mathrm{B} + \boldsymbol{w}_\mathrm{B}$ with $\boldsymbol{x}_\mathrm{B}, \boldsymbol{v}_\mathrm{B}, \boldsymbol{w}_\mathrm{B} \in \mathbb{R}^{n_\mathrm{B}} \subseteq \delta\Omega$ and $n_\mathrm{B} < n_\mathrm{x}$.

Therefore, functions $\boldsymbol{g}_\mathrm{u}$ and $\boldsymbol{g}_0$ are only calculated for surface states $\boldsymbol{w}_\mathrm{B}$ and $\boldsymbol{v}_\mathrm{B}$, that are affected by boundary conditions. Both vectors can be constructed from reduced system states with binary matrix $\boldsymbol{H} \in \mathbb{R}^{n_\mathrm{B}\times n_\mathrm{x}}$

$$\boldsymbol{w}_\mathrm{B} = \boldsymbol{H}\boldsymbol{w}, \;\; \boldsymbol{v}_\mathrm{B} = \boldsymbol{H}\boldsymbol{v}. \tag{13}$$

Furthermore, functions $\boldsymbol{g}_\mathrm{u} : \mathbb{R}^{n_\mathrm{B}} \times \mathbb{R}^{n_\mathrm{u}} \times \mathbb{R}^{n_\mathrm{p}} \to \mathbb{R}^{q_\mathrm{u}}$ and $\boldsymbol{g}_0 : \mathbb{R}^{n_\mathrm{B}} \times \mathbb{R}^{n_\mathrm{p}} \to \mathbb{R}^{q_0}$ are only recalculated, if one surface state changes more than a predefined threshold T_thres. This means they remain constant between correction-steps i and $i+1$ and hence, superposition of both dynamics is still a valid approach. Note that these steps are not necessarily equidistant in time. Main advantage of this formulation is a tune-able balancing between accuracy and computation time. A low threshold leads to more frequently updated operating point corrections and hence, a good accuracy but higher computation cost. When a higher execution trigger threshold is set, deviation towards actual operating point gets larger, leading to lower accuracy but lower computation time. If an infinite threshold is set, the evaluation is a truly linear simulation and deviation is equal to linearization and MOR error. Eventually, order reduced description for initial condition response is formulated as

$$\dot{\tilde{\boldsymbol{w}}} = \tilde{\boldsymbol{A}}_0\,\tilde{\boldsymbol{w}} + \tilde{\boldsymbol{X}}_0\boldsymbol{\gamma} + \boldsymbol{g}_0(\boldsymbol{w}_{\mathrm{B},i}, \boldsymbol{p}_i), \quad \tilde{\boldsymbol{w}}(0) = \boldsymbol{0}, \tag{14}$$

with projection matrices $\boldsymbol{V}_0, \boldsymbol{W}_0 \in \mathbb{R}^{n_\mathrm{x}\times q_0}$ calculated by IRKA, state vector $\tilde{\boldsymbol{w}} \in \mathbb{R}^{q_0}$, system matrix $\tilde{\boldsymbol{A}}_0 \in \mathbb{R}^{q_0\times q_0}$, $\tilde{\boldsymbol{A}}_0 = \boldsymbol{W}_0^\mathrm{T}\boldsymbol{A}\boldsymbol{V}_0$, matrix $\tilde{\boldsymbol{X}}_0 \in \mathbb{R}^{q_0\times n_0}$, $\tilde{\boldsymbol{X}}_0 = \boldsymbol{W}_0^\mathrm{T}\boldsymbol{X}_0$, and corrector function

$$\boldsymbol{g}_0 = \boldsymbol{W}_0^\mathrm{T}\boldsymbol{A}\boldsymbol{H}^\mathrm{T}|_{(\boldsymbol{p}_i - \boldsymbol{p}_0)}\boldsymbol{w}_{\mathrm{B},i}\,. \tag{15}$$

The formulation for load dynamic is

$$\dot{\tilde{\boldsymbol{v}}} = \tilde{\boldsymbol{A}}_\mathrm{u}\,\tilde{\boldsymbol{v}} + \tilde{\boldsymbol{B}}\,\boldsymbol{u} + \boldsymbol{g}_u(\boldsymbol{v}_{\mathrm{B},i}, \boldsymbol{u}_i, \boldsymbol{p}_i), \quad \tilde{\boldsymbol{v}}(0) = \boldsymbol{0}, \tag{16}$$

with $\boldsymbol{V}_\mathrm{u}, \boldsymbol{W}_\mathrm{u} \in \mathbb{R}^{n_\mathrm{x}\times q_\mathrm{u}}$, state vector $\tilde{\boldsymbol{v}} \in \mathbb{R}^{q_\mathrm{u}}$, system matrix $\tilde{\boldsymbol{A}}_\mathrm{u} = \boldsymbol{W}_\mathrm{u}^\mathrm{T}\boldsymbol{A}\boldsymbol{V}_\mathrm{u}$, $\tilde{\boldsymbol{A}}_\mathrm{u} \in \mathbb{R}^{q_\mathrm{u}\times q_\mathrm{u}}$, input matrix $\tilde{\boldsymbol{B}} = \boldsymbol{W}_\mathrm{u}^\mathrm{T}\boldsymbol{B}$, $\tilde{\boldsymbol{B}} \in \mathbb{R}^{q_\mathrm{u}\times n_\mathrm{u}}$, and corrector function

$$\boldsymbol{g}_\mathrm{u} = \boldsymbol{W}_\mathrm{u}^\mathrm{T}\boldsymbol{A}\boldsymbol{H}^\mathrm{T}|_{(\boldsymbol{p}_i - \boldsymbol{p}_0)}\boldsymbol{v}_{\mathrm{B},i} + \boldsymbol{W}_\mathrm{u}^\mathrm{T}\boldsymbol{B}|_{(\boldsymbol{p}_i - \boldsymbol{p}_0)}\,\boldsymbol{u}_i\,. \tag{17}$$

Temperature values at sensor positions are calculated from reduced states

$$\tilde{\boldsymbol{T}}_\mathrm{S} = \tilde{\boldsymbol{C}}_\mathrm{u}\,\tilde{\boldsymbol{v}} + \tilde{\boldsymbol{C}}_0\,\tilde{\boldsymbol{w}}, \tag{18}$$

with output matrix $\tilde{\boldsymbol{C}}_\mathrm{u} = \boldsymbol{C}_\mathrm{u}\boldsymbol{V}_\mathrm{u}$, $\tilde{\boldsymbol{C}}_\mathrm{u} \in \mathbb{R}^{n_\mathrm{y}\times q_\mathrm{u}}$ and output matrix $\tilde{\boldsymbol{C}}_0 = \boldsymbol{C}_0\boldsymbol{V}_0$, $\tilde{\boldsymbol{C}}_0 \in \mathbb{R}^{n_\mathrm{y}\times q_0}$.

The differential equations (14) and (16) preserve physical interpretation of parameters $\boldsymbol{p}$, despite model order reduction. Therefore, parameter values can be adjusted without time-consuming recalculation of projection matrices. This allows for accurate and computation efficient simulation of thermal systems, affected by temperature dependent boundary conditions. This approach is used to first perform parameter identification from measurements and subsequently use verified models for prediction.

2.2 Evaluation Methods

Guaranteed execution times are crucial for real-time applications. Since full order ordinary differential equations, derived from FEA, entail very high execution times, model order reduction has been applied. In order to achieve a sufficiently accurate and fast simulation, several options can be set. The chosen reduced dimensions (q_u, q_0) for each dynamic is dependent on system complexity. This can results in a conflict in objectives, because a higher order most likely leads to higher conformity with original full

order system but simultaneously entails a higher execution time. For the rubber specimen original system scale is $n_{\text{rubber}} = 5271$ and reduced orders are set to $q_{\text{u,rubber}} = 18$ and $q_{0,\text{rubber}} = 19$, whereas for the tire model, $n_{\text{tire}} = 7167$ is reduced to $q_{\text{u,tire}} = 18$ and $q_{0,\text{tire}} = 19$. Reduced dimensions are empirically determined so that over all state deviation throughout the whole cross-section (all states n_{x}) over all time steps k

$$\Delta x_{\text{RMS}} = \sqrt{\frac{1}{n_{\text{x}}} \sum_{j=1}^{n_{\text{x}}} \frac{1}{k} \sum_{i=1}^{k} (\boldsymbol{x}_{i,j} - \boldsymbol{V}\tilde{\boldsymbol{x}}_{i,j})^2} \tag{19}$$

is below 0.5 K. This error criterion is used to further evaluate accuracy of execution algorithms. Besides model order, time steps and choice of solver impact computation effort. Therefore, explicit algorithms such as Euler, Heun, classic RungeKutta, and RKDP method of Dormand and Prince (1980) as well as implicit Euler and implicit trapezoid method are compared in regard to numeric stability, accuracy and sample time. Moreover, function calls of g_{u}, g_0 from Equations (15) and (17) have the highest impact on computation costs, since dimension of boundary condition affected surface states n_{B} is higher than the reduced orders. All simulations are performed on an Optiplex 9020, Dual-Core Intel Core i5-4690 3.5 GHz, 32 GB 1600 MHz DDR3 memory, Windows 10, Dell Inc., Round Rock, TX, USA.

3. RESULTS

The two mentioned models are used to conduct experiments regarding accuracy and computation time in regard to model order reduction, time discretization and solver type. In Section 3.1 a reduced thermal model of a tire cross-section is compared to a full order FEA model. Section 3.2 describes parameterization of a rectangular rubber slab model. Real measurement data from an exemplary curing cycle is used to verify the modeling approach. Subsequently, the model is used for real-time prediction.

3.1 Real-time execution of tire model

The half tire cross-section model from Figure 1b is used to evaluate execution parameters and solving algorithm for real-time prediction of large scale thermal models. A full order thermal FEA is performed in ANSYS Mechanical with sample time $h_{\text{ANSYS}} = 0.1\,\text{s}$ and is used as a ground truth. The tire model consists of multiple components from different materials and complex geometries. Therefore, it is a suitable benchmark for proposed prediction method. Figure 2 depicts a sample curing process for the tire. Subsequent to a heating phase ($t_{\text{heat}} = 10$ minutes), cool down begins and is simulated for another 35 minutes. During heating process, no convective or radiative boundary conditions occur, since the tire is enclosed in a mold. Therefore, a simple linear model can be reduced with classical linear model order reduction algorithm rational Krylov. Hence, absolute deviation at sensor position as well as deviation over all tire states is very low and is not further investigated in this work. After ten minutes, nonlinear conditions occur, requiring use of previously proposed method. Deviation at sensor positions is below 1 K during whole cool down. Furthermore, absolute deviation over time for all states is depicted in Figure 2. At each time step state deviation is modeled as a normal distribution and mean, min/max and tolerance within double standard deviation (2σ) is shown. The reduced order model was solved with implicit Euler method, sample time $h = 0.1$s, and boundary conditions are updated with a set threshold of $T_{\text{thres}} = 10\,\text{K}$. It can be stated, that this modeling approach and its configuration is suitable for sufficiently accurate cure status determination. To achieve real-time requirements, accuracy and computation time in regard to threshold T_{thres} have to be investigated. As previously mentioned, all following results are only calculated for the cool down phase. Figure 3 depicts the influence of chosen trigger threshold on computation time t_{calc} and state deviation Δx_{RMS}. If the threshold is set to a minimum, film coefficients are updated for every time steps leading to a computation time of t_{calc} =3 min with an accuracy of $\Delta x_{\text{RMS}} = 0.46\,\text{K}$. For a maximum threshold, no corrections are made and the simulation is truly linear. Computation time for this case is $t_{\text{calc}} = 0.3\,\text{s}$ with an accuracy of $\Delta x_{\text{RMS}} = 1.6\,\text{K}$. A suitable balancing between accuracy and computation time is a threshold between 1 and 10 K. Further results are shown in Table 1. FEA is used as ground truth and entails the highest computation time of about 28 minutes. With rising threshold T_{thres}, number of execution of the corrective term n_{fcalls} decreases and hence, computation time decreases until linear case is matched. However, state deviation between full and reduced order model increases.

Table 1. Tire Model Results

T_{thres} in K	$\Delta \boldsymbol{x}_{\text{RMS}}$ in K	n_{fcalls}	t_{calc} in s
FEA	Ground Truth		∼28 min
0	0.46	8000	195
0.1	0.463	1198	29
0.5	0.468	288	7.2
1	0.475	148	3.9
2	0.49	76	2.2
5	0.54	31	1.2
10	0.68	16	0.8
20	1.04	8	0.6
linear model	1.7	0	0.4

Furthermore, choice of solving algorithm and sample time can effect simulation outcome. Threshold is set to $T_{\text{thres}} = 1\,\text{K}$ for all further evaluations regarding solving algorithms. Computation times t_{calc} and state deviation $\Delta \boldsymbol{x}_{\text{RMS}}$ for explicit algorithms such as Euler, Heun, Runge and classic Runge-Kutta with varying sample time h are depicted in Figure 4. For all methods sample time h has no great influence on accuracy, but all solvers show instable behaviour above $h \geq 1\,\text{s}$ and are not suitable for this approach. Although implicit solver have a higher computational effort solving differential equations, algorithm convergence is not affected by choice of sample time. As it is shown in Figure 5 higher sample times can be chosen, to further reduce computation time. Overall, implicit trapezoid method shows the best performance in regard to accuracy and time.

3.2 Parameter Identification from Experiment

In a first experiment a rubber slab is heated with a subsequent cooling process to mimic a complete curing

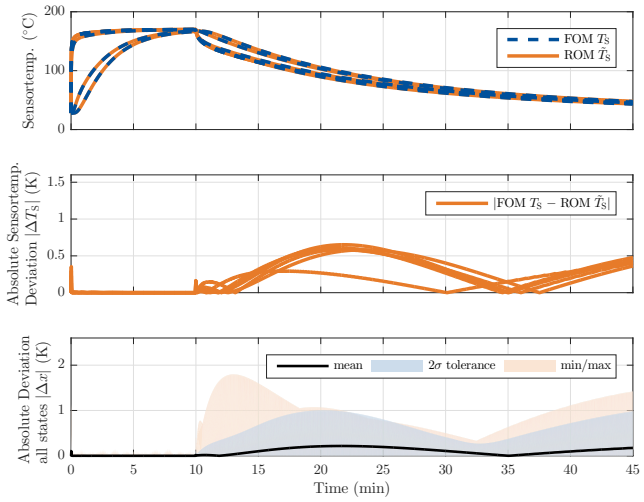

Fig. 2. Comparison between full order tire cross-section model (FOM) from FEA and order reduced expression (ROM)

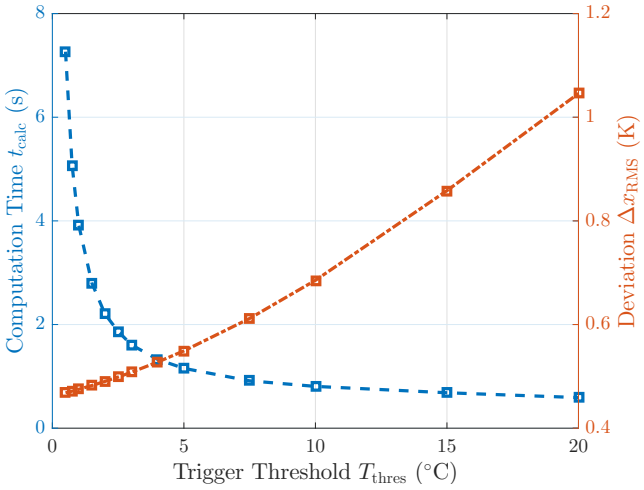

Fig. 3. Influence of trigger threshold T_{thres} on computation time t_{calc} and state deviation Δx_{RMS}

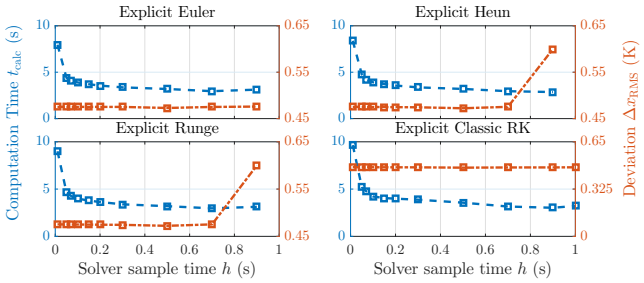

Fig. 4. Influence of explicit solving algorithm's sample time h on accuracy Δx_{RMS} and computation time t_{calc}

procedure. Two sensors are embedded in order to monitor the temperature in the middle of the cross-section (see also Figure 1a). Sensor positions are measured using computed tomography images, since small deviations in positions can cause high errors, due to the low thermal conductivity of rubber compounds. During the heating phase, the rubber is placed between two molds as introduced by Bossel-mann et al. (2017). In the subsequent cooling phase, the specimen is exposed to natural convection in a ventilated

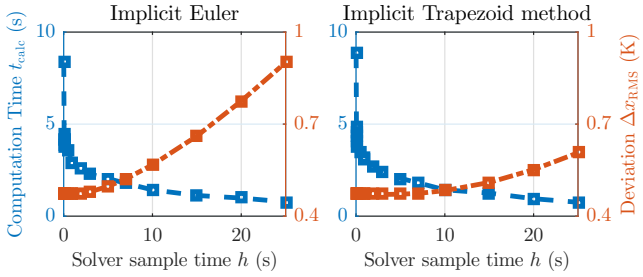

Fig. 5. Influence of implicit solving algorithm's sample time h on accuracy Δx_{RMS} and computation time t_{calc}

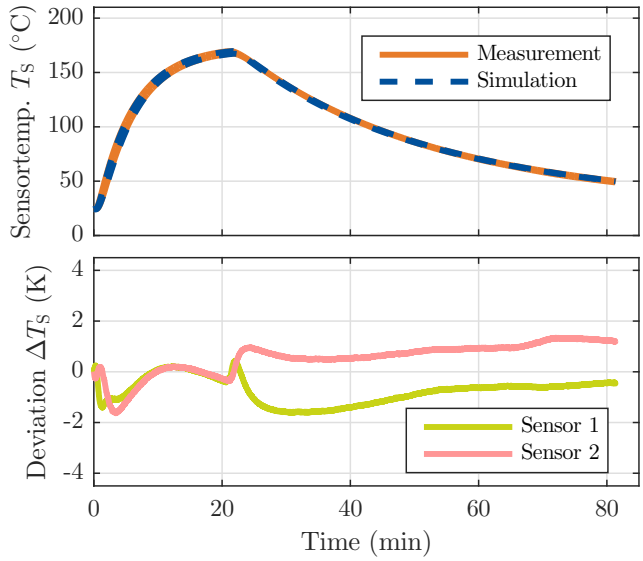

Fig. 6. Sensor-temperature curves of real-time prediction with verified rubber slab model compared to real measurements during a sample curing process

laboratory. Multiple heating cycles with different duration and mold temperatures are recorded. The measured sensor temperatures are used for identification of thermal boundary conditions, during the cooling at ambient temperature. Therefore, parameters $\boldsymbol{p}$ including film coefficients are identified by minimizing deviation between model and measurement with the approach of Frank et al. (2019).

3.3 Real-time prediction of rubber specimen cooling phase

In this section previously identified boundary condition parameters are used for real-time prediction of a rubber slab sample curing process. Furthermore, execution parameters $T_{\text{thres}} = 1\,\text{K}$, sample time $h = 1\,\text{s}$ and implicit trapezoid method as solving algorithm are set. Simulation execution time is below 1 s and thus, suitable for task cycle times of 1 s and higher. Figure 6 depicts measured sensor temperatures for a curing process at 170 °C mold temperature and simulation results from verified real-time capable rubber slab model. Overall deviation does not exceed 2 K. Residual errors can be affiliated to uncontrollable air flows in the laboratory, uncertain material properties and reduction errors. However, it can be stated that proposed modeling approach is suitable to approximate process behaviour online in real-time.

4. CONCLUSION

In this manuscript a modeling approach for real-time capable thermal long-term prediction is presented. A special remark is given to large system scale, that can be entailed by finite element analysis of complex geometries or materials. Main advantage is the use of model reduction methods in order to enable fine spatial discretization in FEA. Moreover, no model simplifications in dimension or linearization are required to deal with state-dependent boundary conditions. The model equations can be directly derived from FEA. New parameter options are added to solve for conflicting goals of computation time and accuracy. Eventually, a compromise is found to successfully perform real-time prediction with a verified thermal model. Predicted temperature distributions over time can be used to calculate cure status at the end of the whole curing process. Frequently executed during heating, it can be utilized to calculate optimum heat duration in regard to varying ambient conditions during cooling. In future work, a state observer will be implemented to adapt real-time models from available sensor measurements. These models and observers can eventually be used for model-based temperature or process control algorithms, which are currently unfeasible approaches due to high system scales and nonlinear influences.

ACKNOWLEDGEMENTS

This work was supported by the German Federal Ministry for Economic Affairs and Energy.

REFERENCES

Advani, S.G. and Sozer, E.M. (2010). *Process Modeling in Composites Manufacturing, Second Edition*. CRC Press, Boca Raton, 2nd ed. edition.

Aleksendrić, D., Carlone, P., and Ćirović, V. (2016). Optimization of the temperature-time curve for the curing process of thermoset matrix composites. *Applied Composite Materials*, 23(5), 1047–1063. doi:10.1007/s10443-016-9499-y.

Beattie, C., Gugercin, S., and Mehrmann, V. (2017). Model reduction for systems with inhomogeneous initial conditions. *Systems Control Letters*, 99, 99–106. doi:10.1016/j.sysconle.2016.11.007.

Benner, P., Ohlberger, M., Cohen, A., and Willcox, K. (2017). *Model Reduction and Approximation*. Society for Industrial and Applied Mathematics, Philadelphia, PA. doi:10.1137/1.9781611974829.

Bosselmann, S., Frank, T., Wielitzka, M., Dagen, M., and Ortmaier, T. (2017). Thermal modeling and decentralized control of mold temperature for a vulcanization test bench. In *2017 IEEE Conference on Control Technology and Applications (CCTA)*, 377–382. doi:10.1109/CCTA.2017.8062491.

Bosselmann, S., Frank, T., Wielitzka, M., and Ortmaier, T. (2018). Optimization of process parameters for rubber curing in relation to vulcanization requirements and energy consumption. In *AIM 2018*, 804–809. IEEE, Piscataway, NJ. doi:10.1109/AIM.2018.8452354.

Dormand, J. and Prince, P. (1980). A family of embedded runge-kutta formulae. *Journal of Computational and Applied Mathematics*, 6(1), 19 – 26. doi:https://doi.org/10.1016/0771-050X(80)90013-3.

Frank, T., Bosselmann, S., Wielitzka, M., and Ortmaier, T. (2018). Computation-efficient simulation of nonlinear thermal boundary conditions for large-scale models. *IEEE Control Systems Letters*, 2(3), 351–356. doi:10.1109/LCSYS.2018.2840428.

Frank, T., Wieting, S., Wielitzka, M., Bosselmann, S., and Ortmaier, T. (2019). Identification of temperature-dependent boundary conditions using mor. *International Journal of Numerical Methods for Heat & Fluid Flow*, ahead-of-print(ahead-of-print), 711. doi:10.1108/HFF-05-2019-0404.

Ghoreishy, M.H.R. (2016). A state-of-the-art review on the mathematical modeling and computer simulation of rubber vulcanization process. *Iranian Polymer Journal*, 25(1), 89–109. doi:10.1007/s13726-015-0405-5.

Giacometto, F., Capelli, F., Romeral, L., Riba, J.R., and Sala, E. (2016). Thermal response estimation in substation connectors using data-driven models. *Advances in Electrical and Computer Engineering*, 16(3), 25–30. doi:10.4316/AECE.2016.03004.

Grimme, E. (1997). Krylov projection methods for model reduction. *Department of Electrical and Computer Engineering, University of Illinois at Urbana-Champaign*.

Gugercin, S., Antoulas, A.C., and Beattie, C. (2008). $\mathcal{H}_2$ model reduction for large-scale linear dynamical systems. *SIAM Journal on Matrix Analysis and Applications*, 30(2), 609–638. doi:10.1137/060666123. URL `https://doi.org/10.1137/060666123`.

Labban, A.E., Mousseau, P., Bailleul, J.L., and Deterre, R. (2010). Optimization of thick rubber part curing cycles. *Inverse Problems in Science and Engineering*, 18(3), 313–340. doi:10.1080/17415971003589517.

Qi, F., Ly, D.A., van der Broeck, C., Yan, D., and de Doncker, R.W. (2016). Model order reduction suitable for online linear parameter-varying thermal models of electric motors. In *2016 IEEE 2nd Annual Southern Power Electronics Conference (SPEC)*, 1–6. IEEE, Piscataway, NJ. doi:10.1109/SPEC.2016.7846147.

Speicher, K., Steinboeck, A., Kugi, A., Wild, D., and Kiefer, T. (2014). Analysis and design of an extended kalman filter for the plate temperature in heavy plate rolling. *Journal of Process Control*, 24(9), 1371–1381. doi:10.1016/j.jprocont.2014.06.004.

Speicher, K., Steinboeck, A., Wild, D., Kiefer, T., and Kugi, A. (2013). Estimation of plate temperatures in hot rolling based on an extended kalman filter. *IFAC Proceedings Volumes*, 46(16), 409–414. doi:10.3182/20130825-4-US-2038.00006.